Low voltage electric potential as a driving force to hinder biofouling in self-supporting carbon nanotube membranes

Chidambaram Thamaraiselvan[a], Avner Ronen[a#], Sofia Lerman[a], Moran Balaish[b], Yair Ein-Eli[b] and Carlos G. Dosoretz[a]*

[a]Faculty of Civil and Environmental Engineering and Grand Water Research Institute, Technion-Israel Institute of Technology, Haifa 3200003, Israel.

[b]Department of Materials Science and Engineering, Technion-Israel Institute of Technology, Haifa 3200003, Israel

[#a]Permanent address: Department of Civil and Environmental Engineering, Temple University, Philadelphia, PA 19122, United States.

*Corresponding author: Civil and Environmental Engineering, Technion-Israel Institute of Technology, Haifa 3200003, Israel. E-mail address: carlosd@technion.ac.il.

Abstract

This study aimed at evaluating the contribution of low voltage electric field, both alternating (AC) and direct (DC) currents, on the prevention of bacterial attachment and cell inactivation to highly electrically conductive self-supporting carbon nanotubes (CNT) membranes at conditions which encourage biofilm formation. A mutant strain of *Pseudomonas putida* S12 was used a model bacterium and either capacitive or resistive electrical circuits and two flow regimes, flow-through and cross-flow filtration, were studied. Major emphasis was placed on AC due to its ability of repulsing and inactivating bacteria. AC voltage at 1.5V, 1 kHz frequency and wave pulse above offset (+0.45) with 100Ω external resistance on the ground side prevented almost completely attachment of bacteria (>98.5%) with concomitant high inactivation (95.3±2.5%) in flow-through regime. AC resulted more effective than DC, both in terms of biofouling reduction compared to cathodic DC and in terms of cell inactivation compared to anodic DC. Although similar trends were observed, a net reduced extent of prevention of bacterial attachment and inactivation was observed in filtration as compared to flow-through regime, which is mainly attributed to the permeate drag force, also supported by theoretical calculations in DC in capacitive mode. Electrochemical impedance spectroscopy analysis suggests a pure resistor behavior in resistance mode compared to involvement of redox reactions in capacitance mode, as source for bacteria detachment and inactivation. Although further optimization is required, electrically polarized CNT membranes offer a viable antibiofouling strategy to hinder biofouling and simplify membrane care during filtration.

Keywords: Biofouling; self-supported CNT membrane; alternating current; bacterial attachment; cell inactivation.

1. Introduction

Biofouling control is considered to be one of the greatest challenges in membrane filtration of water (Flemming et al., 1997). Carbon nanotubes (CNTs) have a great potential for applications in water and wastewater treatment due to their inherent antibacterial characteristics, physical and chemical properties and high electrical conductivity (Das et al., 2014; Upadhyayula and Gadhamshetty, 2010). Composite membranes embedded with CNTs display good degree of intrinsic antibacterial activity, dependent on the CNT size, structure and attached chemical groups (Kang et al., 2008; Li et al., 2008).

Electrical current has been described to influence bacterial adhesion to conductive surfaces in medical and industrial applications. High electrical field (kV/cm range) is known to inactivate bacteria and yeasts (Hamilton and Sale, 1967; Hülsheger et al., 1981, 1983) and has been described for surface sanitation (Harrison et al., 1997; Marx et al., 2011). In the last decade there is a growing interest in applying low electrical fields (mV/cm range) to control bacterial adhesion and biofilm formation on conductive surfaces, such as surgical stainless steel and gold, platinum and indium-tin oxide electrodes, especially for detachment of bacteria (Poortinga et al., 2001; Busalmen and De Sánchez, 2001; van der Borden et al., 2004; Pérez-Roa et al., 2006; Hong et al., 2008; Kang et al., 2011; Shim et al., 2011). In the water treatment field, the application of a low alternating current (AC) potential (1.5 V, square wave) on a conductive NF membrane to control biofilm formation was reported (De Lannoy et al., 2013). An electrically conductive feed spacer was studied to test bacterial detachment from fouled membranes applying 1V electrical potential (positive, negative, and alternating) (Baek et al., 2014). Similarly, bacterial detachment from electrically conducting membranes when applying a direct current (DC) potential of 1.5V was shown (Ronen et al., 2015a), with inactivation of the remaining attached bacteria (32±2.1% cathodic; 67±3.6% anodic).

Both AC and DC have been studied for their capabilities to detach, prevent attachment and inactivate bacteria cells, including the specific role of anodic, cathodic and block currents. The extent of detachment was significant with cathodic DC but most residual attached bacteria remained alive (Hong et al., 2008). In contrast, when an anodic DC was applied very low bacterial detachment was found, although bacteria that remained on the surface became inactive with time (Hong et al., 2008). For AC, both detachment and inactivation were effectively observed concomitantly (Baek et al., 2014; Hong et al., 2008; van der Borden et al., 2005), therefore, combining bacterial detachment similarly to negative DC coupled with bactericidal influence as in positive DC, making it most suitable for biofilm control (Shim et al., 2011). Increasing frequency also had a positive influence in enhanced bacterial detachment in AC (van der Borden et al., 2005). DC, when cathodic potential, i.e., negative current is applied to a solid surface, electrostatic and electrophoretic forces (vertical) dominate the bacterial detachment (Poortinga et al., 2001). When applying anodic potential, i.e., positive current, the bonding between the solid and bacterial surfaces loosens due to electroosmotic forces (parallel), and the bacteria could be washed off to some extent by increasing shear rate (Hong et al., 2008).

The mechanism of inactivation can be explained by direct oxidation, which damages the cell membrane and indirect oxidation due to generation of biocides such as hydroxyl radicals, free chlorine and hydrogen peroxide (Asadi and Torkaman, 2014; Jeong et al., 2007). For example, the inactivation of bacteria was correlated with the generation of low concentrations of H_2O_2 in a electrochemical system (Istanbullu et al., 2012; Ronen et al., 2015a). Initial attachment is dominated by van der Waals, electrostatic, hydrophilic/hydrophobic forces, and bacteria surface properties following the classical Derjaguin, Landau, Verwey and Overbeek (DLVO) theory (An and Friedman, 1998; Hermansson, 1999; Poortinga et al., 2002; Dorobantu et al., 2009). An additional dominating force in crossflow filtration systems is the

94 permeate drag force, which increases bacterial adhesion to the membranes and eventually
95 leads to biofouling (Eshed et al., 2008).
96 Despite many studies on bacteria detachment on conductive surfaces, no reports focused on
97 prevention of the initial attachment, and moreover, most if not all studies were performed
98 with resting cells cultures. Only very few studies have been done with water filtration
99 membranes (De Lannoy et al., 2013; Ronen et al., 2015a). Applying electric potential on
100 membrane modules to control biofouling can be potentially applied to highly conductive
101 membranes. Moreover, the optimization of suitable alternating electric field for biofilm
102 control has not yet been reported, while previous studies were performed in capacitive
103 configuration with aid of electrolytes. The present research studied the prevention of initial
104 bacterial attachment to electrically conductive self-supporting CNT membranes at conditions
105 encouraging bacterial growth, in two flow regimes, flow through and cross-flow filtration.
106 Both AC and DC in either capacitive or resistive electrical configuration were studied.
107 Resistive mode has been study as an alternative for the application of CNT membranes for
108 filtration of low electrical conductivity media, such wastewater effluents. Major emphasis
109 was placed on AC due to its ability of repulsing and inactivating bacteria.

110 **2. Materials and Methods**

111 ***2.1 Membranes***

112 Self-supporting CNT membranes were supplied by Tortech Nano Fibers (TNF). CNT fibers
113 were fabricated by direct spinning from chemical vapor deposition (CVD) synthesis using a
114 liquid source of carbon and an iron nanocatalyst, as described by Li et al. (2004). The
115 molecular weight cut off the membranes is in the tight ultrafiltration range (Thamaraiselvan
116 et al., 2017). Their structure provides the CNT membrane with high strength, increased
117 thermal stability (up to 400°C), wide chemical resistance, high permeability and high electric

conductivity (≥40,000 S/m). The electrical resistance of the membranes was measured with a LCR 4300 meter (Wayne Kerr Electronics), values reported are for wet conditions.

2.2 Microorganism

A mutant strain of *Pseudomonas putida* S12 (ATCC 700801) was used as a model organism. Preservation, sub-culturing and inoculum preparation were performed in Luria Bertani (LB) broth containing 50 μg/mL kanamycin, as a previously described (Eshed et al., 2008). A single Gram (-) species biofilm was used in order to simplify the test system and provide a mean for easier tracking of biofilm development. Inoculum was harvested to an average optical density of approx. OD_{600}=0.7.

2.3. Electrical membrane biofouling system (EMBS)

2.3.1. Description of the experimental system and operation conditions

The biofouling inhibition activity was tested in a flow-through electrical membrane biofouling system (EMBS). It comprised six flow-through membrane cells with a set of electrodes each, operating in continuous mode with internal recirculation through two reactors, with every three flow-cells connected to one reactor. Fig. 1 shows a schematic diagram of a typical set up of the EMBS under different electrical circuits (detailed information is available in supplementary information). Details of the flow-through cell are included in Fig. S1.

All cells were equipped with pressure gauges and pressure transducers (inlet and outlet pressure) and flow-valve controller, and operated at a low linear flow velocity of about 0.02 m/s. The recirculation reactors (40 mL capacity each) were kept at a retention time of approx. 20 min, below the doubling time of the model bacterium at such growth conditions to encourage biofilm formation (Eshed et al., 2008). Feed consisted of a solution of sterile LB medium diluted in place (1:250) with filtered tap water (0.8/0.2 μm filter, Pall) supplied by means of a peristaltic pump (Cole-Parmer) (Fig. 1). Total organic carbon (TOC)

concentration in the feed stream upon dilution was ~20 mg/L. Each reactor was equipped with a thermocouple for temperature monitoring. Prior to experiments, the membranes (35 cm^2 area) were assembled in the cleaned flow cells, washed with filter-sterilized water for an hour and then equilibrated with the feed solution. Next, the system was inoculated to a bacterial concentration of 10^4 CFU/mL and kept for 1 h in closed circulation and then operated in continuous mode with recirculation. Upon inoculation cells were connected to the electrical field as indicated. Due to the biofilm encouraging conditions (i.e., organic loading rate, inoculum concentration, suspended bacteria retention time) experiments duration was set to approx. 72 hours.

Experiments were performed in two modes: (i) flow-through conditions, meaning no transmembrane pressure gradient (no permeation); (ii) cross-flow filtration mode at 10 psi (~69 kPa) pressure. Pressure, temperature and the electric potential were continuously monitored and controlled using LabVIEW. At the end of the experiments, the membranes were removed, thoroughly washed with sterile saline solution and taken for microscopic analysis. All components of the system were cleaned with 70% ethanol and rinsed with distilled water. In experiments performed in full cross-flow mode with filtration, fouling development was monitored by measuring the normalized permeate flux decrease during the experiment. The initial flux was measured just before inoculation. The normalized flux was defined as the actual flux divided by the initial flux. Unless otherwise stated, experiments were repeated at least 3 times. Microscopic analyses were made at least in three random areas on the surface of the membrane and results presented are representative.

2.3.2. Electrical set up and conditions

DC, generated by a power supply (GW Instek, GPD-3303s) or AC electric field, generated by a dual channel arbitrary function generator-AFG (GW Instek, AFG-2225), were applied as indicated. A high-voltage (0-60 V), high-current (0-5 A) amplifier (OPA548, Texas

Instruments) was connected to each channel of the AC function generator, to deliver the required power output to the system. A square wave pulse at offset V_{pp} (millivolt peak to peak) or above (positive pulse)/below (negative pulse) offset was applied for AC, at a duty ratio of 50%. The range of conditions investigated include AC voltage from 0.3-6.0V at frequencies ranging from 10 Hz-10 kHz. DC was applied in a voltage range of 0.6-3.0V. Two electrical circuits were explored for both currents. One was in resistive mode using an external resistance in the range of 10-200Ω. The other was in capacitive mode with feed solution supplemented with 50 mM NaCl to enhance the electrical conductivity between electrodes. Voltage drop at was measured at the membrane connectors using a DSO-X 2004A Oscilloscope (Digital Storage).

The electrical current (I, mA) applied to the membranes was calculated as a function of the voltage (V) and total resistance (R, Ω), I = V/R, where the total resistance, R, is the sum of the external or medium resistance and membrane resistance. The electrical power consumption (P, W) was calculated as

$$P = V \times I \qquad \text{(Eq. 1)}$$

Surface temperature developed on the membranes connected in resistive mode was measured with VariCAM HiRe IR camera (Panasonic) and LIT 8 IR thermometer. Measurements were performed at controlled ambient air conditions (25±1℃) and data reported is after at least 10 min of electricity applied.

2.4 Analytical Techniques

2.4.1 High Resolution-Scanning Electron Microscope (HR-SEM)

HR-SEM was performed in a Carl Zeiss Ultra-Plus FEG-SEM. Samples were fixed with glutaraldehyde 3% (v/v) and dehydrated using a cold ethanol gradient at 4ºC (Eshed et al., 2008). Prior to imaging, samples were sputter coated with carbon.

2.4.2 Confocal Laser Scanning Microscope (CLSM)

193 CLSM imaging was performed using a Carl Zeiss CLSM (LSM 510 META) with a ×63
194 water-dipping objective. In order to visualize dead/live bacterial attachment, the membrane
195 samples were stained with dead/live staining (Invitrogen-Molecular Probes): 5 µM Syto 9
196 (S34854) and 30 µM propidium iodide (P4170) (Ronen et al., 2013).
197 Image analysis software Imaris 7.7.2 (Bitplane) was used to analyze the dead/live stained
198 CLSM images and quantify the amount of biofilm in terms of specific biovolume (BF_v, μm^3
199 per 100 μm^2); total biovolume was calculated as the sum of both fields. The theoretical
200 number of bacteria (TN_b) within the 3-D structure of the biofilm was calculated estimating the
201 volume of a single bacterium (V_b) as follows (Eq. 2):

202 $$TN_b = BF_v / V_b \ \text{(cell/100 } \mu m^2\text{)} \qquad \text{(Eq. 2)}$$

203 V_b was estimated according to Baldwin and Bankston (1988):

204 $$V_b = \pi r^2 (\tfrac{4}{3} r + l - 2r) \qquad \text{(Eq. 3)}$$

205 based on an average size of an individual cell of *P. putida* of 1.16±0.1 µm length (l) and 0.5
206 µm radius (r) (Ronen et al., 2015b). All z-sections were processed and flattened into a single
207 overlaying layer using Image J (7.7.2win 64). For each analysis, the threshold value was
208 adjusted to highlight the biofilm. The size of each image processed was 85 µm×85 µm.
209 *2.4.3. Electrochemical impedance spectroscopy (EIS)*
210 Potentiostatic EIS was carried out over a frequency range of 1 Hz-100 kHz (0.01V amplitude,
211 sinusoidal wave, VSP-Biologic Science Instruments). Measurements were conducted in a
212 two-electrode cell configuration in resistance and capacitance modes under flow-through
213 conditions, using 1:250 diluted (in tap water) LB medium as is (0 mM NaCl, EC= 635
214 µS/cm) or supplemented with 50 (EC=5,400 µS/cm) and 150 (EC=16,000 µS/cm) mM NaCl.
215 Anodic potentials of 0, 0.45 and 0.9V were applied and Bode plots and complex plane
216 impedance plots under all conditions tested were generated.
217 *2.4.4. Other analytical techniques*

Zeta potential of bacterial suspensions was measured in a 10 mM KCl solution (ZetaSizer Nano-ZS Malvern). Total organic carbon was measured in a TOC-V_{CPH} analyzer (Shimadzu). X-ray photoelectron spectroscopy (XPS) analysis was performed using a Thermo VG-Scientific - Sigma probe system with a monochromatic Al Kα at 1486.6 eV source and a hemispherical electron energy analyzer.

3. Results

3.1 Influence of electrical current in resistive mode on biofouling control

The effect of AC, i.e., polarizing electric field, in resistive mode on the attachment of bacteria on CNT membranes and biofilm formation was first thoroughly studied in flow-through regime in order to find the most effective operational conditions.

The influence of AC frequency in the range of 10 Hz-10 kHz at $1.8V_{pp}$ (at offset) is presented in Fig. 2. As frequency increased antibiofouling (and cell inactivation) gradually increased as depicted by the decrease of bacterial cells attached, reaching the most significant reduction between 10 to 100 Hz, with an almost asymptotic value at 1 kHz. After 72 h of exposure only sporadic cells could be observed on the membranes in all range of frequencies studied in contrast to a relatively dense biofilm observed in the control membranes (11.4±1.2 μm). As can be further seen in Fig. 2, due to the voltage drop along the membrane when connecting it in resistive mode and being the solely resistance, a high (phase) and low (ground) potential sides were noticeable. At the lower frequencies (10 and 100 Hz), the bacterial attachment to the ground side of the CNT membrane was somewhat higher than the phase side, however, no differences between both sides of the membrane were noticed in the kHz range. Increasing the frequency above 10 kHz decreased the amplitude of the electric wave and the antibiofouling effect and inactivation became less effective. The amplitude at a constant AC potential of an electric circuit, at which the total energy is constant, decreases with the

increase of frequency in order to conserve the energy output. Further experiments were thus performed at a frequency of 1 kHz.

In order to reduce the voltage drop along the membrane and decrease the energy expenditure, the effect of an external resistance connected to the ground side of the electric circuit at a constant AC potential of $1.8V_{pp}$, at offset and 1 kHz, was then studied in the range of 0-200Ω. Please note the intrinsic CNT membrane resistance in the electrical circuit was 0.53±0.12Ω. The results are presented in Fig. 3. The addition of an external resistance not only reduced potential drop along the membrane, which behaved as a resistor within the resistive circuit, but also enhanced the prevention of bacterial attachment on the membranes applying the same potential. Indeed, an almost 4-fold decrease of cells attachment (1452.5±240.0 to 345.7±26.8 total cells/100 μm^2) was obtained increasing the external resistance from 0 to 200Ω. However, inactivation decreased with increasing resistance (41.4±7.3 to 19.1±2.8%, respectively), most probably due to current reduction by increasing resistance. Attachment of cells was dominant in the control with most of them in living state (93.2±5.5%). Further experiments were performed with an external resistance of 100Ω.

To further evaluate the antibiofouling/inactivation capabilities of AC in resistive mode, wave pulse shifts above (+0.45, positive potential) and below (-0.45, negative potential) offset were tested comparatively with potential at offset. A constant AC potential at 1 kHz frequency and 100Ω external resistance was applied, meaning -0.9 to +0.9V at offset ($1.8V_{pp}$), 0 to 1.8V above offset and -1.8 to 0V below offset (Fig. 4). Shifting the wave pulse above offset reduced bacterial attachment about 2-fold, from 512.4±32.6 at offset to 228.7±017.4 total cells/100 μm^2 above offset while increased cell inactivation about 4 times (13.6±4.2 to 56.2±9.6%, respectively). Remarkably, shifting the wave pulse below offset resulted somewhat less effective, yielding 427.1±35.2 attached bacteria per 100 μm^2 and 7.3±0.6% inactivation. Again, compared to a relatively dense biofilm layer on the control

membranes (9.1±1.2 μm thickness; 4972.6±313.1 attached cells per 100 μm^2), only sporadic single cells were detected under the electrical field (see Fig. 4). Further experiments were carried out with wave pulse above offset.

Finally, the influence of the AC voltage in resistive mode on antibiofouling capabilities on the CNT membranes was studied in the range of 0.3-1.5V at the most efficient conditions, namely 1 kHz frequency, 100Ω external resistance and wave pulse above the offset (Fig. 5). As clearly seen, increasing the intensity of the electrical field gradually reduced bacterial cells attachment practically completely with a concomitant inactivation of attached bacteria, reaching 95.3±2.5% at 1.5V. Due to the presence of the external resistance and potential above offset both ends of the membrane displayed similar bacterial rejection in all cases.

For comparison, DC potential in resistive mode with a 100Ω external resistance was tested in the voltage range of 0.6-1.5V (Table 1). Increasing the DC potential resulted in an increased prevention of bacterial attachment (~8 fold at 0.6V and ~25 fold at 0.9V to about 300 fold at 1.5V) along with moderate inactivation of attached bacteria (2.4, 22.8 and 29.3%, respectively, relative to the control).

Although a similar trend of attachment was observed in resistive mode in both DC and AC at the same electrical conditions, markedly higher cell inactivation was noticed for AC, i.e., 95% compared to ~29% in DC (compare Fig. 5 and Table 1). Electrostatic rejection and oxidation, either direct or indirect, are both favorable in AC field due to the polarizing current. All in all these results emphasize the advantage of the polarizing current both, on preventing cell attachment and enhancing inactivation.

3.2 Influence of electrical current in capacitive mode on biofouling control

The influence of AC and DC electric fields through capacitive mode was tested under flow-through conditions using growth medium supplemented with 50 mM NaCl.

The effect of AC studied in the range of 0-4.5V above offset is presented in Fig. 6. A relatively dense 3-D biofilm was developed on the control membranes (10.3±1.3 μm) and most attached bacteria (5536.7±560.1 cell/100 μm^2) were in living state (98.3±0.5%). With the increase of the applied electrical potential attached bacteria appeared mostly as sporadic cells in monolayer distribution whose number decreased exponentially at an average rate of 0.9% per 0.001V as the relative rate of inactivation did (0.8 %/0.001V). The increase of dead cells numbers as a result of the increase of the applied potential (16.5±1.0% at 1.0V, 71.2±5.2% at 3.0V and 80.1±5.6% at 4.5V) suggests bacterial inactivation due to oxidation (see Fig. 6). The change in slope increasing the applied potential suggests electrical limitation, most probably due to the electrolyte concentration. HRSEM micrographs displayed a similar trend, decline in number of bacteria attached as the applied electrical potential increased (Fig. 6, middle panel). Damaged cells could be seen at 4.5V possibly due to direct oxidation.

For comparative purposes, the effect of DC electrical potential form 0.9 up to 3.0V in capacitive mode was studied in either cathodic or anodic configuration (Table 2). Compared to a dense biofilm in the control membrane (11.5±1.5 μm thickness), a relatively less dense biofilm (7.4±0.9 μm thickness) was evident at low anodic potential (0.9V) in contrast to almost complete prevention of bacterial attachment at 0.9-3.0V. Decrease of attached bacteria while increasing cathodic potential indicates electrostatic repulsion (see Table 2). However, at difference to AC only a slight inactivation effect could be observed with increasing DC cathodic potential.

Summarizing this part, although both AC and cathodic DC displayed similar antibiofouling activity in capacitive mode, inactivation of AC was markedly superior. Even though anodic DC and AC displayed close related inactivation potential, the former was not effective as the attachment was still dominant. The higher potentials needed for both currents in capacitive

316 mode in comparison to resistive, highlight the reliance of the capacitive system on the
317 electrical conductivity of the medium.
318 ***3.3 Influence of polarized electrical potential on biofouling control in crossflow filtration***
319 ***mode***
320 To evaluate the influence of AC field on the antibiofouling activity of the CNT self-
321 supporting membranes in filtration mode, experiments in both, growing (fed with diluted LB-
322 medium) and non-growing conditions (fed with saline solution), were performed. AC was
323 applied in resistive mode in the voltage range of 0-4.5V at 1 kHz frequency, 100Ω external
324 resistance and square wave pulse above offset (+0.45). For reference, 1.5V DC both anodic
325 and cathodic in capacitive mode were tested.
326 The results in growing conditions are presented in Table 3. A very dense and developed
327 biofilm (thickness of approx. 22 μm) was observed in the control membrane, almost two-fold
328 thicker than that observed in the flow-through controls. This disparity may be attributed to
329 the permeate drag force towards the membrane which in conjunction with intensive biofilm-
330 forming conditions applied counteracted the bacterial rejection of the electrical field.
331 Although in the presence of the electrical field a reduced biofouling layer was observed,
332 which decreased with the increase of the electrical potential, still a defined biofilm rather than
333 sporadic deposition of single cells was observed which was also depicted by negligible effect
334 on the permeation rate of the membrane compared to the control. Nevertheless, inactivation
335 of attached cells increased as function of the electrical potential applied for AC and anodic
336 DC, again, AC potential resulted more effective than anodic or cathodic DC potentials (see
337 Table 3).
338 In order to analyze more in detail the effect of the permeate drag force in presence of the
339 electrical field, a set of cross-flow filtration experiments of 12 h duration was performed at
340 non-growing conditions with sterile saline after inoculation with 10^7 CFU/mL *P. putida*. As

expected, no significant inactivation of bacteria was observed in the control with no current applied (96.5±2.7% remained viable) whereas as the electrical potential increased both the total number of attached bacteria and residual viable bacteria decreased gradually (Table 4). Almost no observed impact on cell viability (94.8±4.2) was seen when applying an AC potential of 1.0V and lower, which correspond to a value below hydrolysis potential of water. These results suggest that inactivation resulted in a bactericidal effect that can be attributed to either direct or indirect oxidation. In in vitro tests performed at electrical conditions similar to those applied in the filtration experiments depicted low H_2O_2 accumulation potential (Fig. S2). Hence, although possibilities for indirect oxidation for inactivation cannot be ruled out, H_2O_2 may not be a decisive factor. The membrane's normalized permeability in cross-flow filtration at non-growing under the electrical field was in good correlation with the microscopic analyses of their surface (Fig. 7). Indeed, while the normalized permeation rate of the control was reduced by approx. 60% after 12 h run, the intensification of the field potential applied along the membranes gradually hindered permeate reduction achieving only 17% reduction at 6.0V.

3.4 Theoretical estimation of electrostatic and drag forces on bacterial attachment in DC field in capacitive mode

In order to describe the deposition of bacterial cells on the membrane surface in the presence of the electrical field, DLVO interactions were considered in combination with bulk and interfacial hydrodynamic interactions. The sum of the bulk and interfacial forces at a given separation distance provides an estimate of the attractive or repulsive force a bacterium might experience. The following forces were taken into consideration: attractive van der Waals (F_{vdW}), modified electrostatic double layer (F_{ES}), cross-flow lift (F_L) and permeation drag (F_D). The net interfacial force (F_T), i.e., the net force between the charged membrane and bacteria, was determined from Eq. 4:

$$F_T = F_D + F_L + F_{ES} + F_{vdW} \quad \text{(Eq. 4)}$$

Due to calculation constraints, only DC field in capacitive mode could be numerically resolved. Calculations are presented in the supplementary information (Eqs. S1-S10). The electrostatic repulsive forces were dominant in cathodic potentials compared to DC anodic potential (Figs. S3 and S4). In flow-through mode, i.e., in the absence of permeate drag force, as the cathodic potential applied on the membrane was increased (from 0.5-3.0V) the calculated primary maximum's distance increased accordingly. In all cases, the overall repulsive forces were in the range of 0.85-1 nN, able to prevent, theoretically, attachment of bacteria or particle to the surface. At this distance, attractive vdW forces are negligible in comparison to the electrostatic repulsive forces (~10^{-3} nN). At lower distances from the membrane, attractive van der Waals interactions become more dominant, depending on the applied potential and eventually leading to adhesion between the bacteria and the charged membrane. These results are in agreement with the low experimental concentrations of bacteria adhered to the membrane surface when a 3V DC cathodic potential was applied (~7%). Electrochemical reactions at cathodic DC potentials > 1.23V which may enhance bacterial detachment were not considered in the theoretical force calculations.

In cross-flow filtration mode, permeate flux adds a dominant drag force leading to the decrease of the net interfacial force, approaching null and negative values at distances of 2.5-5.4 nm according to the applied potential (Fig. S4). The permeate drag force not only changes the distance of the primary maximum but also decreases the overall repulsive force value. Indeed, the influence of the directing drag force imposed by the permeate flux in cross-flow mode compared to transport of cell towards the surface by random flow pattern in flow-through mode can be drawn from the experimental bacterial attachment data of the control membranes, i.e., 0V (9275.4±236.7 and 2724.2±249 cell/100 μm^2, respectively), in line with previous reports (Eshed et al., 2008; Ronen et al., 2015a). Further experimental data depicted

391 bacterial attachment to the membranes surface even when a cathodic potential of 1.5V was
392 applied (5973.4±311.1 cell/100 μm^2), although bacterial concentration decreased with the
393 increasing of applied potential as expected (Table 3, bottom lines). The difference between
394 the experimental and theoretical results of repulsive forces may due to the estimation of the
395 permeate force according to Goren et al. (1973) where the hydrodynamic correction factor
396 may change the permeate drag force significantly. In addition, all calculation refers to inert
397 particles, i.e., bacteria with no motility abilities, while 'real' bacteria can react with the
398 surrounding environment (e.g., motility, pili) and 'swim' towards the membrane surface.

399 ***3.5 Electrochemical impedance spectroscopy analysis***

400 Bode plots and complex plane impedance plots of EIS data generated under different solution
401 concentrations and different applied constant voltages are presented in Figs. S5 and S6 for
402 resistance and capacitance modes, respectively.

403 When no supplemental electrolyte was added to the diluted LB medium (0 mM NaCl), a
404 distinct behavior of a pure inductance with only an imaginary impedance component was
405 evident at higher frequencies (100 kHz<f<1 kHz) and a pure resistance behavior was
406 observed at the lower frequency range (<1 kHz). At a frequency of 1 kHz the CNT membrane
407 was AC-frequency independent and purely behaved as a resistor with a zero-imaginary
408 impedance. At frequencies >1 kHz and even higher upon increase in NaCl concentrations, a
409 current-voltage phase separation occurred in the positive region indicating an inductive
410 behavior.

411 When medium was supplemented with electrolyte (50 and 150 mM NaCl), a new
412 intermediate frequency range was evident (1 kHz>f>10 kHz) with a decrease of (|Z|),
413 indicating that the total impedance of the fabric not only originated from the resistive
414 reactance, but also from a capacitive (when phase angle was negative) or an inductive
415 reactance (when phase angle was positive), or both. The existence of a capacitance behavior

around 1 kHz, observed mainly at high salt concentrations, was followed by a dramatic increase in absolute impedance of the system at frequencies > 10 kHz due to inductance reactance, as manifested in positive phase shift values, alongside negative imaginary impedance components. The capacitive mode configuration is discussed in the supplementary information (Fig. S6).

To test whether CNT degradation takes places upon oxidation in resistive mode, XPS analysis was carried out. The composition, C1s high resolution spectra and deconvolution lines denote minor changes before and after run (Table S1), implying minor deterioration of the CNT structure. In order to assess Ohmic effect and its possible implication on membrane oxidation, temperature development on the membranes connected in resistive mode was measured (Fig. S7 and Table S2). No measurable temperature change as function of voltage was found was found on the membranes surface in either AC or DC with external resistor, depicting negligible heat generation (heat dissipation most probably took place at the external resistor). Moreover, minor changes in conductivity of membrane subjected to electric field for 72 h was noticed compared with the control membranes, regardless of the voltage applied (Fig. S8).

4. Discussion

This study aimed at clarifying the contribution of low voltage electric field with emphasis on polarizing current with respect to attachment, detachment and inactivation of bacteria on charged CNT membranes in flowing regime in growing conditions with emphasis on microporous filtration of wastewater effluents. Primary focus of other studies were mostly on detachment of non-growing/resting bacteria adhered to conductive surfaces, either membranes or electrodes. Limited information was reported on growing conditions and all previous studies were conducted in capacitive mode (De Lannoy et al., 2013; Hong et al., 2008; Ronen et al., 2015a). The present study explored the effect of both capacitive and

441 resistive with external resistance circuits, both in terms of prevention of attachment and
442 inactivation. A summary of attachment, detachment and inactivation of bacteria in
443 conducting surfaces under flow conditions is presented in Table S3.
444 AC resulted more effective than DC, both in terms of biofouling reduction compared to
445 cathodic DC and in terms of cell inactivation compared to anodic DC, either in resistive or
446 capacitive modes. Hence, the electrostatic repulsion combined with direct oxidation seems
447 the dominant mechanism in polarizing current, involving the advantages of anodic oxidation
448 and cathodic electrostatic repulsion (Hong et al., 2008; Van Der Borden et al., 2005). Both
449 AC and cathodic DC electric fields, either in resistive or capacitive modes, suppressed
450 bacterial attachment to higher extent than previous studies (Hong et al., 2008). However, an
451 exact comparison is not possible because of the different experimental set-ups and conditions.
452 The influence of electric currents on prevention of bacterial attachment can be summarized as
453 follows: in capacitive mode AC $\geq$ DC cathodic $\gg$ DC anodic and in resistive mode AC > DC.
454 Polarization of membrane with electric field imposed a strong negative charge to the CNT
455 membrane in AC and cathodic DC, which resulted in a repulsive electrostatic interaction with
456 negatively charged bacteria cells. The thicknesses of the double layer and, in consequence,
457 the influence of the electrostatic repulsion on the bacterial attachment are dependent on the
458 ionic strength (Busalmen and De Sánchez, 2001; Poortinga et al., 2001). When increasing the
459 ionic strength, interaction energy between negatively polarized CNT and bacteria are
460 repulsive at shorter distance and become attractive at distances larger than 5 nm. The
461 shielding of electrostatic repulsion can slightly increase bacterial attachment at lower
462 potential. These observations suggest a higher reliance of capacitive circuits in preventing
463 bacterial attachment on the ionic strength of the medium treated, as well as distance between
464 poles, i.e., feed channel, compared to resistive circuits with external resistance.

Regarding inactivation in capacitive mode, the mechanism is more complex when comparing AC and DC. According to Jeong et al. (2007), initial inactivation occurs rapidly at beginning of electrolysis most probably due to electrosorption of negatively charged *E. coli* cells to the anode surface, followed by a direct electron transfer reaction. Secondary inactivation elapses slow but steady as electrolysis continues, mainly by the action of reactive oxygen species generated from water such as hydroxyl radical. Although applied voltages above 1V can cause water dissociation or formation of active chlorine (Liu et al. 1997; Speight et al., 2005), this phenomenon readily occurs when DC is applied, but it is minimized with AC in the kHz range for water splitting and 50 Hz for chlorine formation (Pérez-Roa et al., 2006). In our work, efficient prevention of bacterial attachment and inactivation were found at increasing frequencies with an optimum 1 kHz-10 kHz. Moreover, a slight increase of inactivation was observed when amplitude shifted above offset and H_2O_2 generation was very low under AC electric field. Although indirect oxidation cannot be ruled out, inactivation might be due to direct electron transfer, disrupting the integrity of the bacterial membrane, leading to a decrease in viability.

In AC resistive mode, the antibiofouling activity was significantly more effective than capacitive mode (compare plots in Figs. 5 and 6), strongly suggesting that low current density was sufficient to both reject and inactivate bacteria. This is in line with a pure resistor behavior derived EIS analysis, indicating a different functionality of the CNT fabric at the relevant frequency range (~1 kHz) and low EC medium. The pure resistance behavior, as opposed to a resistance-capacitance reactant is predicted to affect the bacteria detachment and deactivation mechanism. Although oxidation processes seem to be the main cause for detachment and loss of viability of bacteria in capacitance mode, only minor oxidation of the CNT surface was observed in resistance mode. Cell inactivation of attached bacteria in resistive mode may be also linked to direct oxidation, as such low current densities at high

490 frequency may be sufficient to infringe charge separation across the bilayer cell membrane,
491 and in turn increase transmembrane potential. This effect may lead local membrane damage,
492 either reversible or irreversibly, that consequently will increase permeability (Barbosa-
493 Canovas et al., 2000; Jiménez-Sánchez et al., 2017). Furthermore, logarithmic growing cells
494 were reported more sensitive to electrical fields than stationary cells whereas square-wave
495 pulses have been described more energy and lethally efficient than exponential pulse
496 (Barbosa-Canovas et al., 2000). Since most other previous studies were performed with non-
497 growing/resting cells in capacitive mode, can explain the higher sensitivity reported here
498 even at low current densities.
499 Due to the function of the CNT as a pure resistor, some contribution of Ohmic heating cannot
500 be completely ruled out as part of a viable detachment and deactivation mechanism in
501 resistive mode. Nevertheless, Ohmic heating at the experimental conditions studied in the
502 presence of an external resistor (low voltage and current) is expected to be very low, as also
503 indicated by temperature measurements on the membrane surface. Furthermore, due to the
504 high recirculation ratio the EMBS system an efficient heat dissipation would be expected.
505 Bacterial cell inactivation due to Ohmic heating is described at electric field strengths above
506 30 V/cm and temperature above 50°C, at a rate proportional to the electrical conductivity of
507 the medium (Jiménez-Sánchez et al., 2017).
508 Generally speaking, composite CNTs films can exhibit resistive, capacitive and in some cases
509 also inductive phases allowing a comprehensive analysis of processes related to electrical
510 double layer (EDL) formation and CNT electro-oxidation mitigation as a function of
511 frequency (Dudchenko et al., 2017). Pure CNT fabrics comprised of chiral tubes may exhibit
512 inductance behaviour at frequencies in the kHz range (Watts et al, 2002). A distinct behavior
513 of a pure inductance with only an imaginary impedance component was evident at the higher
514 frequencies (≥10 kHz) and higher salinities (≥5,400 µS/cm) and a pure resistance observed

515 at the lower frequency range (<1 kHz) in resistive mode. At the conditions applied, low EC of
516 the medium (635 µS/cm), low voltage 0.3-1.5V and moderate frequency (1 kHz) one cannot
517 rule out double layer charging, but if there is it will be very minor.
518 The net reduced extent of prevention of bacterial attachment and inactivation found in
519 filtration mode is mainly attributed to the permeate drag force (Eshed et al., 2008; Ronen et
520 al., 2015a). Since harsh biofouling promoting conditions were applied in the present study,
521 the conditions for the electrical field still need to be optimized in filtration mode.
522 Nevertheless, in terms of prevention of attachment and inactivation, similar trends were
523 observed under cross-flow filtration as in flow-through mode. The population of bacteria in
524 real pretreated feedwater will be at least two orders of magnitude lower of that tested here
525 and crossflow velocity about one order of magnitude higher enhancing repulsive lift and
526 shear rate forces. Thus, biofouling control by AC is expected to be feasible adapting the
527 electric field to the bacterial population and nutrients present in the feedwater.
528 **5. Conclusions**
529 This study contributed to clarify the antibiofouling performance of low voltage electric field,
530 in flow conditions, evaluated by attachment, detachment and inactivation of bacteria on self-
531 supporting, highly conductive CNT membranes. Both electrostatic and bactericidal effects
532 seem to be involved. AC resulted better than DC electric field since it supports both
533 prevention of attachment and inactivation. Resistive mode circuit with external resistance
534 displays effective antibiofouling capabilities regardless of the electrical conductivity of the
535 medium yet at very low power consumption (6.4 W/m^2 applying 1.5V, 100 Ω). Although the
536 strength of the electrical field needs to be optimized to overcome the permeate drag forces,
537 electrically polarized, self-supported CNT membranes offer a viable strategy to hinder
538 biofouling and simplify membrane care during filtration.
539

Acknowledgements

This work was funded by the NOFAR program, Ministry of Commerce, Israel and supported in part at the Technion by a Technion-Guangdong fellowship. Russell Berrie Nanotechnology Institute (RBNI) at Technion is gratefully acknowledged for its support. Authors gratefully acknowledged the Tortech Nano Fibers Ltd. for CNTs laminates fabrication. We thank Ariel Weinshtock for his assistance with the setup of the electrical system of the flow-through cells.

References

An, Y.H., Friedman, R.J., 1998. Concise review of mechanisms of bacterial adhesion to biomaterial surfaces. J. Biomed. Mater. Res. 43, 338–348.

Asadi, M.R., Torkaman, G., 2014. Bacterial inhibition by electrical stimulation. Adv. Wound Care (New Rochelle) 3, 91–97.

Baek, Y., Yoon, H., Shim, S., Choi, J., Yoon, J., 2014. Electroconductive feed spacer as a tool for biofouling control in a membrane system for water treatment. Environ. Sci. Technol. Lett. 1, 179–184.

Barbosa-Canovas, G.V., Pierson, M.D., Zhang, Q.H., Schaffner, D.W. 2000. Pulsed electric fields. J. Food Sci. (Suppl. s8) 65, 65–79.

Busalmen, J.P., De Sánchez, S.R., 2001. Adhesion of *Pseudomonas fluorescens* (ATCC 17552) to nonpolarized and polarized thin films of gold. Appl. Environ. Microbiol. 67, 3188–3194.

Das, R., Ali, M.E., Hamid, S.B.A., Ramakrishna, S., Chowdhury, Z.Z., 2014. Carbon nanotube membranes for water purification: A bright future in water desalination. Desalination 336, 97–109.

De Lannoy, C.F., Jassby, D., Gloe, K., Gordon, A.D., Wiesner, M.R., 2013. Aquatic

biofouling prevention by electrically charged nanocomposite polymer thin film membranes. Environ. Sci. Technol. 47, 2760–2768.

Dorobantu, L.S., Bhattacharjee, S., Foght, J.M., Gray, M.R., 2009. Analysis of force interactions between AFM tips and hydrophobic bacteria using DLVO theory. Langmuir 25, 6968–6976.

Dudchenko, A.V., Chen, C., Cardenas, A., Rolf, J. and Jassby, D. 2017. Frequency-dependent stability of CNT Joule heaters in ionizable media and desalination processes. Nat. Nanotechnol. 12, 557-563.

Eshed, L., Yaron, S., Dosoretz, C.G., 2008. Effect of permeate drag force on the development of a biofouling layer in a pressure-driven membrane separation system. Appl. Environ. Microbiol. 74, 7338–7347.

Flemming, H.C., Schaule, G., Griebe, T., Schmitt, J., Tamachkiarowa, A., 1997. Biofouling - the Achilles heel of membrane processes. Desalination 113, 215–225.

Goren, S.L., 1973. The hydrodynamic force resisting the approach of a sphere to a plane wall in slip flow. J. Colloid Interface Sci. 44, 356–360.

Hamilton, W.A., Sale, A.J.H., 1967. Effects of high electric fields on microorganisms: II. Mechanism of action of the lethal effect. Biochim. Biophys. Acta 148, 789–800.

Harrison, S.L., Barbosa-Cánovas, G. V, Swanson, B.G., 1997. *Saccharomyces cerevisiae* structural changes induced by pulsed electric field treatment. Lebensm.-Wiss. u.-Technol. 30, 236–240.

Hermansson, M., 1999. The DLVO theory in microbial adhesion. Colloids Surf. B 14, 105–119.

Hong, S.H., Jeong, J., Shim, S., Kang, H., Kwon, S., Ahn, K.H., Yoon, J., 2008. Effect of electric currents on bacterial detachment and inactivation. Biotechnol. Bioeng. 100, 379–386.

590 Hülsheger, H., Potel, J., Niemann, E.G., 1981. Killing of bacteria with electric pulses of high
591 field strength. Radiat. Environ. Biophys. 20, 53–65.
592 Hülsheger, H., Potel, J., Niemann, E.G., 1983. Electric field effects on bacteria and yeast
593 cells. Radiat. Environ. Biophys. 22, 149–162.
594 Istanbullu, O., Babauta, J., Duc Nguyen, H., Beyenal, H., 2012. Electrochemical biofilm
595 control: mechanism of action. Biofouling 28, 769–78.
596 Jeong, J., Kim, J.Y., Cho, M., Choi, W., Yoon, J., 2007. Inactivation of *Escherichia coli* in
597 the electrochemical disinfection process using a Pt anode. Chemosphere 67, 652–659.
598 Jiménez-Sánchez, C., Lozano-Sánchez, J., Segura-Carretero, A., Fernández-Gutiérrez, A.,
599 2017. Alternatives to conventional thermal treatments in fruit-juice processing. Part 1:
600 Techniques and applications, Critical Rev. Food Sci. Nutr. 57, 501-523.
601 Kang, H., Shim, S., Lee, S.J., Yoon, J., Ahn, K.H., 2011. Bacterial translational motion on
602 the electrode surface under anodic electric field. Environ. Sci. Technol. 45, 5769–5774.
603 Kang, S., Herzberg, M., Rodrigues, D.F., Elimelech, M., 2008. Antibacterial effects of carbon
604 nanotubes: size does matter! Langmuir 24, 6409–6413.
605 Li, Q., Mahendra, S., Lyon, D.Y., Brunet, L., Liga, M.V., 2008. Antimicrobial nanomaterials
606 for water disinfection and microbial control: potential applications and implications.
607 Water Res. 42, 4591–4602.
608 Li, Y.L., Kinloch, I.A., Windle, A.H., 2004. Direct spinning of carbon nanotube fibers from
609 chemical vapor deposition synthesis. Science 304, 276–278.
610 Liu, W.K., Brown, M.R.W., Elliott, T.S.J., 1997. Mechanisms of the bactericidal activity of
611 low amperage electric current (DC). J. Antimicrob. Chemother. 39, 687–695.
612 Marx, G., Moody, A., Bermúdez-Aguirre, D., 2011. A comparative study on the structure of
613 *Saccharomyces cerevisiae* under nonthermal technologies: High hydrostatic pressure,
614 pulsed electric fields and thermo-sonication. Int. J. Food Microbiol. 151, 327–337.

615 Pérez-Roa, R.E., Tompkins, D.T., Paulose, M., Grimes, C.A., Anderson, M.A., Noguera,
616 D.R., 2006. Effects of localised, low-voltage pulsed electric fields on the development
617 and inhibition of *Pseudomonas aeruginosa* biofilms. Biofouling 22, 383–390.
618 Poortinga, A.T., Bos, R., Norde, W., Busscher, H.J., 2002. Electric double layer interactions
619 in bacterial adhesion to surfaces, Surf. Sci. Rep. 47, 1-32.
620 Poortinga, A.T., Smit, J., Van Der Mei, H.C., Busscher, H.J., 2001. Electric field induced
621 desorption of bacteria from a conditioning film covered substratum. Biotechnol. Bioeng.
622 76, 395–399.
623 Ronen, A., Duan, W., Wheeldon, I., Walker, S.L., Jassby, D., 2015a. Microbial attachment
624 inhibition through low voltage electrochemical reactions on electrically conducting
625 membranes. Environ. Sci. Technol. 49, 12741–12750.
626 Ronen, A., Lerman, S., Ramon, G.Z., Dosoretz, C.G., 2015b. Experimental characterization
627 and numerical simulation of the anti-biofuling activity of nanosilver-modified feed
628 spacers in membrane filtration. J. Memb. Sci. 475, 320–329.
629 Ronen, A., Semiat, R., Dosoretz, C.G., 2013. Impact of ZnO embedded feed spacer on
630 biofilm development in membrane systems. Water Res. 47, 6628–6638.
631 Shim, S., Hong, S.H., Tak, Y., Yoon, J., 2011. Prevention of *Pseudomonas aeruginosa*
632 adhesion by electric currents. Biofouling 27, 217–224.
633 Speight, J., Lange, N.A., Dean, J.A., 2005. Lange's Handbook of Chemistry (16th Edition).
634 EBook, McGraw-Hill Professional Publishing, pp. 1,382.
635 Thamaraiselvan, C., Lerman, S., Weinfeld-Cohen, K., Dosoretz, C.G., 2017. Characterization
636 of a support-free carbon nanotube-microporous membrane for water and wastewater
637 filtration. Desalination under review.
638 Upadhyayula, V.K.K., Gadhamshetty, V., 2010. Appreciating the role of carbon nanotube
639 composites in preventing biofouling and promoting biofilms on material surfaces in

environmental engineering: A review. Biotechnol. Adv. 28, 802–816.

van der Borden, A J., van der Mei, H.C., Busscher, H.J., 2004. Electric-current-induced detachment of *Staphylococcus epidermidis* strains from surgical stainless steel. J. Biomed. Mater. Res. B. Appl. Biomater. 68, 160–164.

van Der Borden, A. J., van Der Mei, H.C., Busscher, H.J., 2005. Electric block current induced detachment from surgical stainless steel and decreased viability of *Staphylococcus epidermidis*. Biomater. 26, 6731–6735.

Watts, P.C.P., Hsu, W.K., Randall, D.P., Kotzeva, V., Chen, G.Z. 2002. Fe-filled carbon nanotubes: nano-electromagnetic inductors. Chem. Mater. 14, 4505-4508.

650 **Figure Legends**

651 **Figure 1.** Schematic diagram of the electrical membrane biofouling system (EMBS) with
652 pressure, temperature and current/voltage monitoring, highlighting feed and permeate flow
653 streams and electrical connections. Cells 1-4 exemplify electrical circuit in resistive mode:
654 1,2-AC and 3,4-DC (1,3 without and 2,4 with external resistance), whereas cell 5 exemplify
655 AC in capacitive mode and cell 6 control (no electricity).

656 **Figure 2.** Effect of AC frequency on bacteria cells attached on the CNT membranes in
657 resistive mode in flow-through regime (growing conditions). Data represent Imaris
658 quantification of CLSM images of dead/live stained biofilm/bacteria attached on the CNT
659 membranes after 72 hours incubation (average±standard deviation of at least 3 replicates).
660 Control, no current. Electrical field conditions were: voltage 0.9V at offset ($1.8V_{pp}$), 50%
661 duty cycle, square wave. Inset show control (no electricity). Current sign shows wave shape
662 and bias.

663 **Figure 3.** Effect of external resistance on bacteria cells attached on the CNT membranes
664 under AC polarizing field in resistive mode in flow-through regime (growing conditions).
665 Data represent Imaris quantification of CLSM images of dead/live stained biofilm/bacteria
666 attached on the CNT membranes after 72 hours incubation (average±standard deviation of at
667 least 3 replicates). Control, no current. Electrical field conditions were: voltage at offset
668 ($1.8V_{pp}$), 1 kHz frequency, 50% duty cycle, square wave. Current sign shows wave shape and
669 bias.

670 **Figure 4.** Effect of AC offset on bacteria cells attached on the CNT membranes in resistive
671 mode in flow-through regime (growing conditions). Data represent Imaris quantification of
672 CLSM images of dead/live stained biofilm/bacteria attached on the CNT membranes after 72
673 hours incubation (average±standard deviation of at least 3 replicates). Control, no current.
674 Electrical field conditions were: 1 kHz frequency, 100Ω external resistance, 50% duty cycle,

675 square wave and 0.9V effective current ($1.8V_{pp}$ at offset; 0.9V at +0.45 above offset; 0.9V at
676 -0.45 below offset). Current signs show wave shape and bias.
677 **Figure 5.** Effect of AC voltage on biofilm control in resistive mode in flow-through regime
678 (growing conditions). Graph: Imaris quantification of CLSM images of dead/live stained
679 biofilm/bacteria attached on the CNT membranes after 72 hours incubation
680 (average±standard deviation of at least 3 replicates). Micrographs: HRSEM images of the
681 CNT membranes after 72 h of incubation; Magnification x30K. Control, no current.
682 Electrical field conditions: frequency 1 kHz, square wave above offset (+0.45), 50% duty
683 cycle, 100 Ω external resistance. Current sign shows wave shape and bias.
684 **Figure 6.** Effect of AC voltage on biofilm control in capacitive mode in flow-through regime
685 (growing conditions). Top: CLSM images of dead/live stained bacteria attached on the
686 membranes after 72 h incubation. Middle: HRSEM images of the CNT membranes after 72 h
687 of incubation. Bottom: Imaris quantification of CLSM images (average±standard deviation of
688 at least 3 replicates). Control, no current. Electrical field conditions were: 1 kHz frequency,
689 square wave above offset (+0.45), 50% duty cycle. Current sign shows wave shape and bias.
690 **Figure 7.** Effect of AC voltage in resistive mode with 100 Ω external resistance on
691 normalized permeability of CNT membranes during 12 h cross-flow filtration with 10^6
692 CFU/ml of *P. putida* S12 in non-growing media (saline). AC was applied at 1 kHz frequency
693 and square wave above offset (+0.45).
694

Table 1. Effect of DC voltage on biofilm control in resistive mode with 100 Ω external resistance in flow-through regime (growing conditions).

Voltage (V)	Attached bacteria (cell/100 μm^2)		Cell inactivation (%)
	Live	Dead	
Control	4067.9±270.2	46.6±2.3	1.1±0.0
0.6	533.2±5.6	12.9±0.9	2.4±0.1
0.9	124.5±20.1	36.7±7.0	23.1±6.0
1.5	10.0±1.8	4.1±1.0	29.4±6.8

*Values represent average±standard deviation of at least 3 replicates of Imaris quantification of biofilm attached on the CNT membranes after 72 h incubation.

Table 2. Effect of DC voltage on biofilm control in capacitive mode in flow-through regime (growing conditions).

Voltage (V)	Attached bacteria (cell/100 μm^2)		Cell inactivation (%)
	Live	Dead	
Control	2491.5±219.6	232.7±29.5	8.5±0.3
0.9 (A)	1574.5±133.5	607.4±28.9	27.9±2.6
0.9 (C)	34.8±7.5	1.1±1.0	3.2±2.9
1.5 (C)	7. 7±1.2	0.9±0.5	10.5±3.7
3.0 (C)	3.2±1.5	1.3±1.0	24.0±11.0

*Values represent average±standard deviation of at least 3 replicates of Imaris quantification of biofilm attached on the membranes after 72 h incubation. (A): anodic current; (C): cathodic current.

Table 3. Effect of electrical potential on biofilm control in cross-flow regime (growing conditions).

Voltage (V)	Attached bacteria (cell/100 μm^2)		Cell inactivation (%)
	Live	Dead	
Control (resistive)	9624.2±280.9	191.4±17.2	1.95±0.2
AC-0.9	6726.7±335.6	218.2±17.9	3.14±0.2
AC-1.5	3852.6±89.2	1892.6±97.6	32.94±1.4
AC-3.0	3054.6±90.6	2596.9±181.1	45.92±2.4
AC-4.5	2097.9±85.7	2318.1±107.3	52.49±0.4
Control (capacitive)	9122.7±214.6	152.7±22.1	1.65±0.3
DC-1.5 (C)	5594.0±268.6	379.4±42.5	6.36±0.7
DC-1.5 (A)	7459.3±1005.8	1950.1±120.1	20.85±2.1

*Values represent average±standard deviation of at least 3 replicates of Imaris quantification of biofilm attached on the membranes after 72 h incubation. AC was applied in resistive mode with 100 Ω external resistance at 1 kHz frequency, square wave above offset (+0.45) in different voltage. (C) cathodic current, (A) anodic current.

Table 4. Effect of AC voltage on biofilm control in resistive mode with 100 Ω external resistance in cross-flow regime (non-growing conditions).

Voltage (V)	Attached bacteria (cell/100 μm^2)		Residual viable bacteria (%)
	Live	Dead	
Control	432.0±15.9	16.4±13.2	96.5±2.7
1.0	410.7±39.5	21.9±17.5	94.8±4.2
3.0	80.8±19.6	128. 5±8.7	38.3±6.2
4.5	24.3±3.4	99.2±25.6	20.2±4.7
6.0	4.8±2.0	21.8±7.0	18.2±7.0

*Values represent average±standard deviation of at least 3 replicates of Imaris quantification of biofilm attached on the membranes after 12 h filtration. AC was applied in resistive mode with 100 Ω external resistance at 1 kHz frequency, square wave above offset (+0.45).

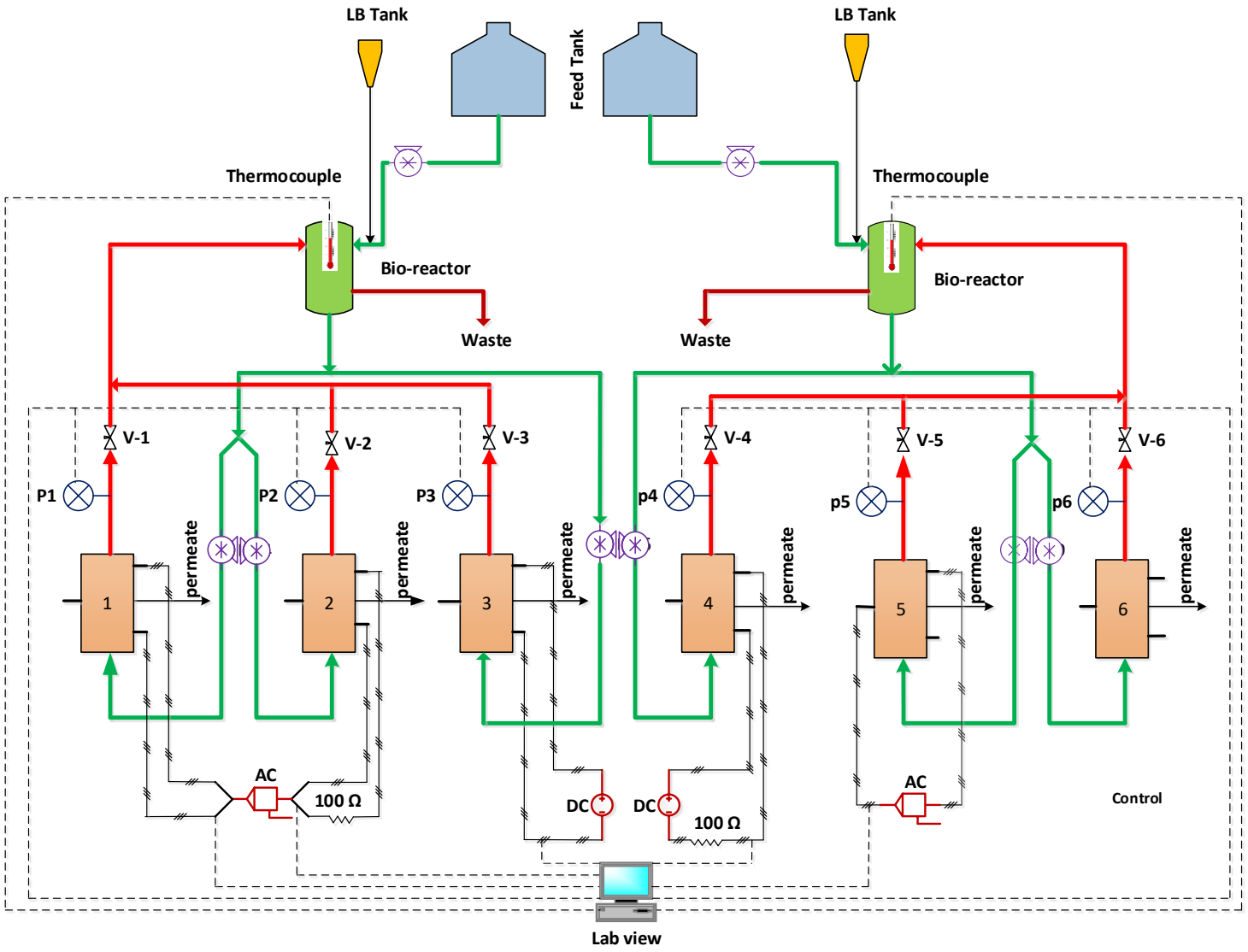
LB Tank
Feed Tank
LB Tank
Thermocouple
Thermocouple
Bio-reactor
Bio-reactor
Waste
Waste
V-1
V-2
V-3
V-4
V-5
V-6
P1
P2
P3
p4
p5
p6
permeate
permeate
permeate
permeate
permeate
permeate
1
2
3
4
5
6
AC
100 Ω
DC
DC
100 Ω
AC
Control
Lab view

Figure 1

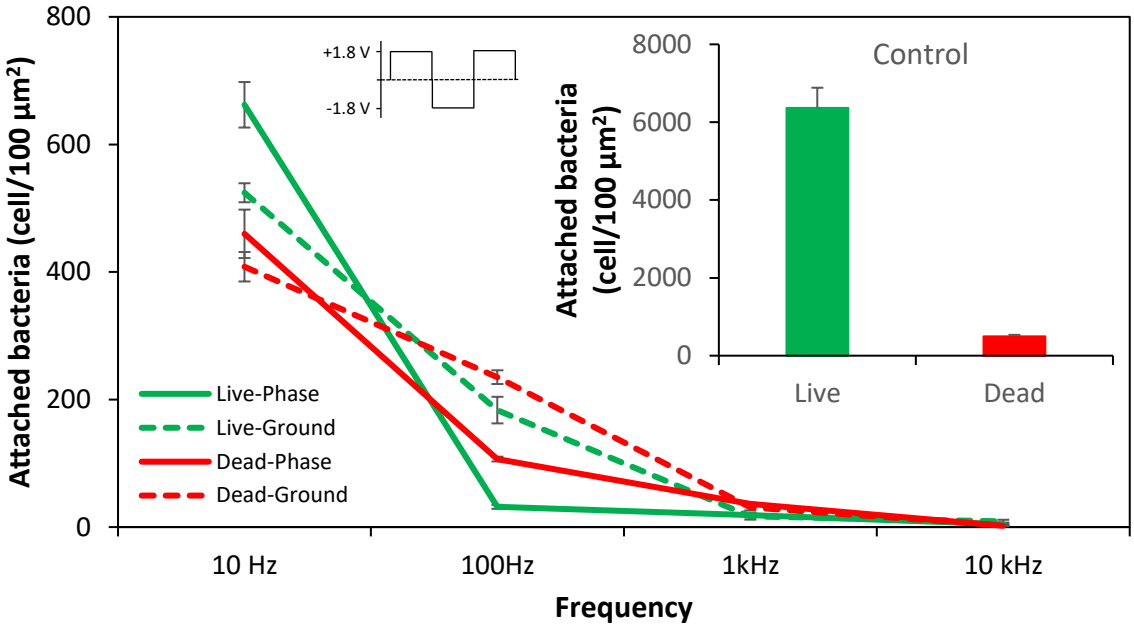
800
600
400
200
0
Attached bacteria (cell/100 µm²)
+1.8 V
-1.8 V
Live-Phase
Live-Ground
Dead-Phase
Dead-Ground
10 Hz
100Hz
1kHz
10 kHz
Frequency
8000
6000
4000
2000
0
Attached bacteria (cell/100 µm²)
Control
Live
Dead

Figure 2

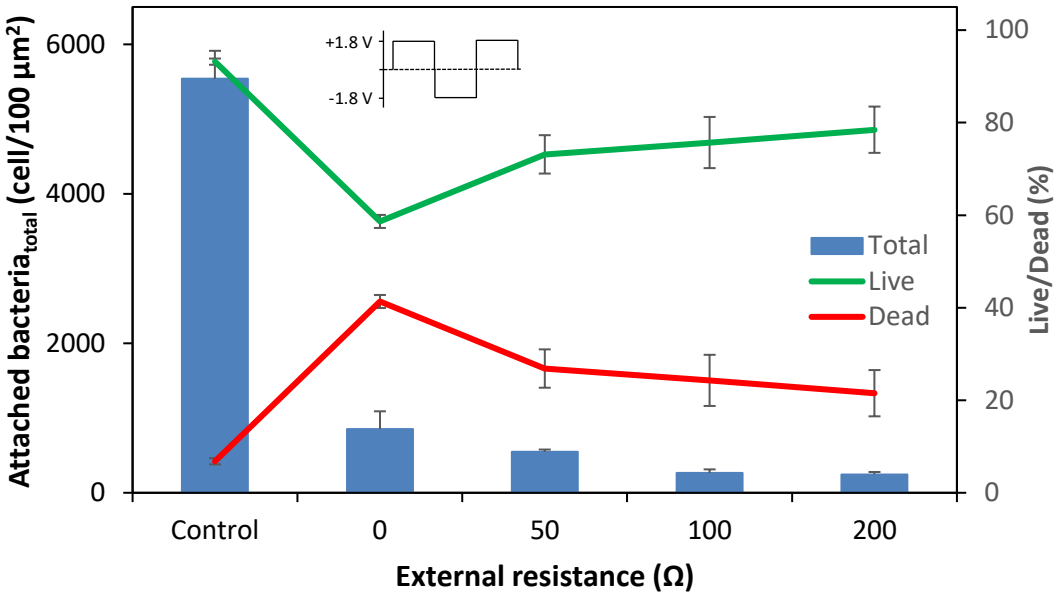
Attached bacteria$_{total}$ (cell/100 µm^2)
6000
4000
2000
0
+1.8 V
-1.8 V
Total
Live
Dead
100
80
60
40
20
0
Live/Dead (%)
Control
0
50
100
200
External resistance (Ω)

Figure 3

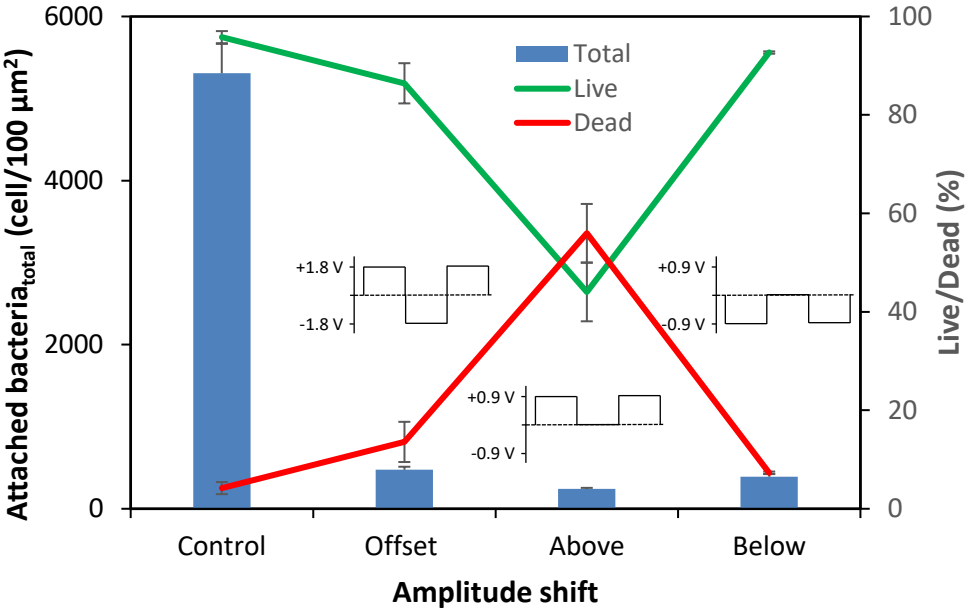
6000
4000
2000
0
100
80
60
40
20
0
Attached bacteria$_{total}$ (cell/100 µm²)
Live/Dead (%)
Total
Live
Dead
+1.8 V
-1.8 V
+0.9 V
-0.9 V
+0.9 V
-0.9 V
Control
Offset
Above
Below
Amplitude shift

Figure 4

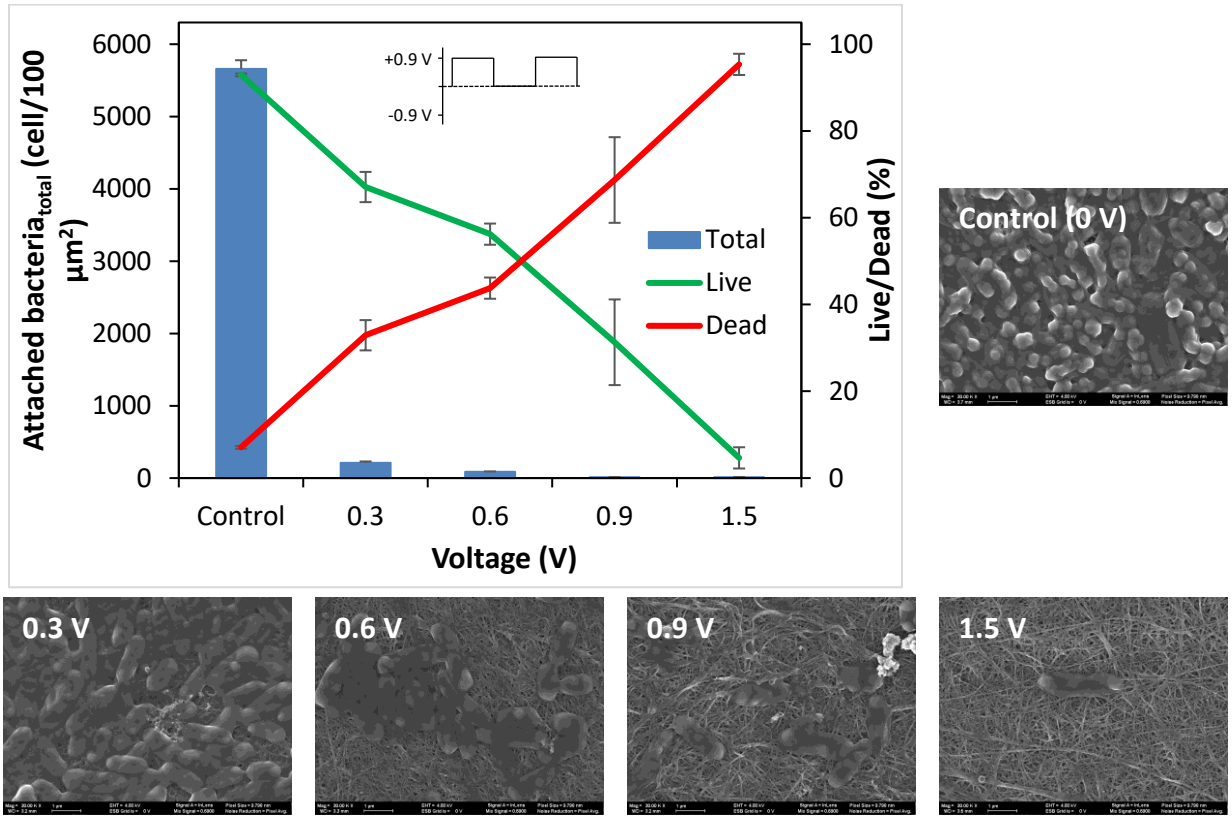
Attached bacteria$_{total}$ (cell/100 μm^2)
6000
5000
4000
3000
2000
1000
0
+0.9 V
-0.9 V
Total
Live
Dead
100
80
60
40
20
0
Live/Dead (%)
Control
0.3
0.6
0.9
1.5
Voltage (V)
Control (0 V)
0.3 V
0.6 V
0.9 V
1.5 V

Figure 5

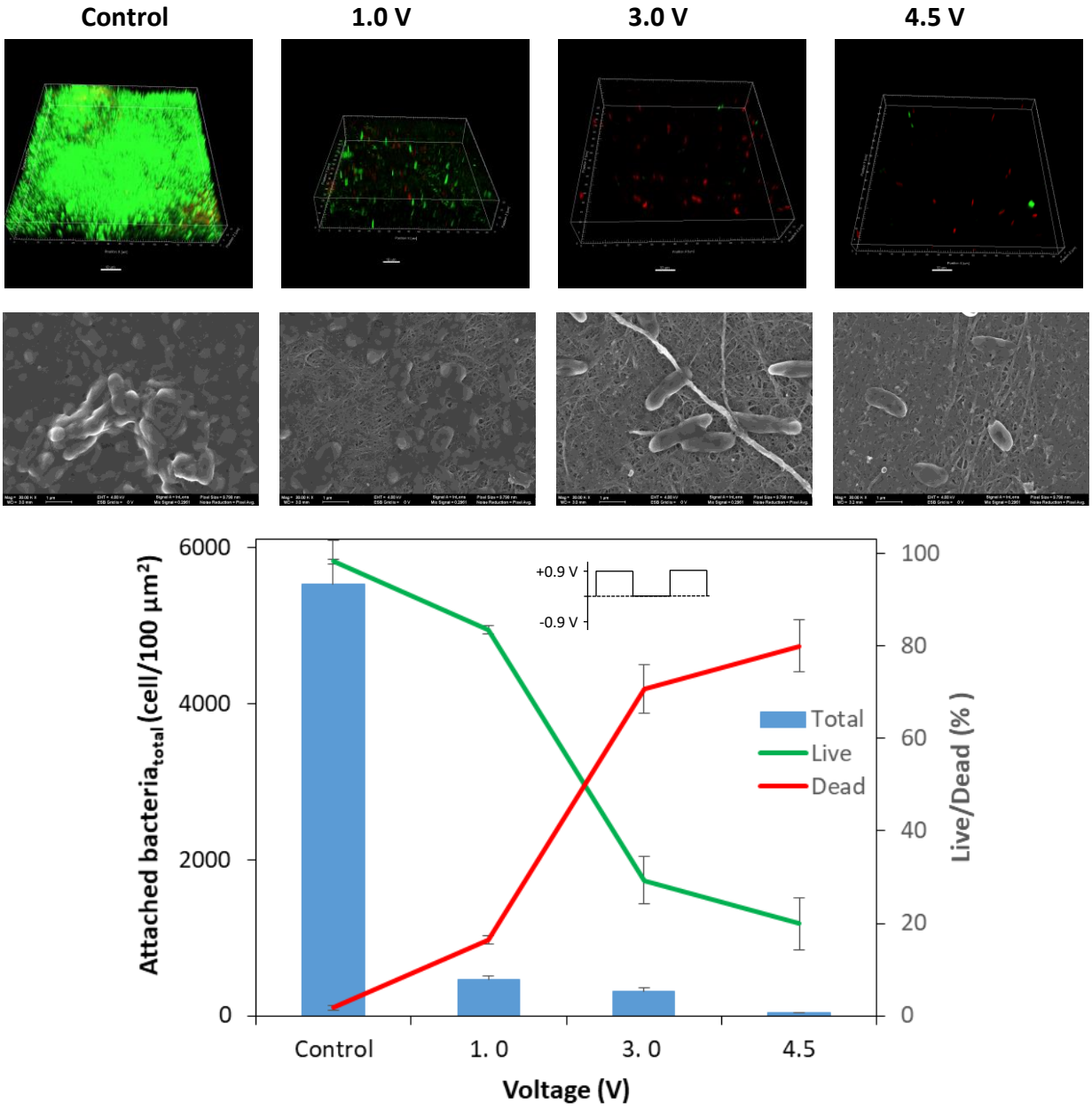
Control
1.0 V
3.0 V
4.5 V
Attached bacteria$_{total}$ (cell/100 μm²)
Live/Dead (%)
+0.9 V
-0.9 V
Total
Live
Dead
Control
1. 0
3. 0
4.5
Voltage (V)

Figure 6

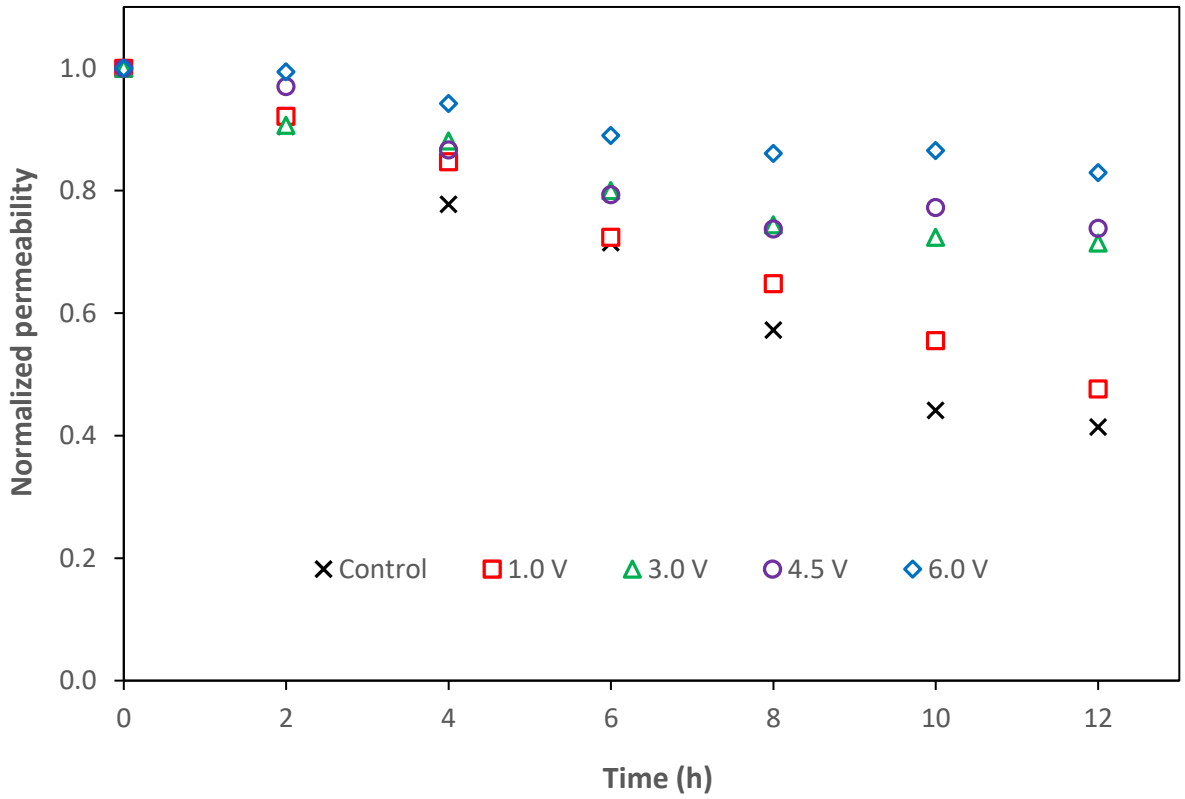
Normalized permeability
1.0
0.8
0.6
0.4
0.2
0.0
0
2
4
6
8
10
12
Time (h)
Control
1.0 V
3.0 V
4.5 V
6.0 V

Figure 7